Materials Research Bulletin 90 (2017) 295–302

Contents lists available at ScienceDirect

Materials Research Bulletin

journal homepage: www.elsevier.com/locate/matresbu

Effect of temperature on the structural characteristics and electrical/dielectric response of nacrite-NaCl nanohybrid material

Nouha Jaafar*, Hafsia Ben Rhaiem, Abdesslem Ben Haj Amara

UR13ES46: Unity of Research of Physics of Lamellar Materials and Hybrid Nano-Materials, University of Carthage, Faculty of Sciences of Bizerte, Zarzouna 7021, Tunisia

ARTICLE INFO

Article history:
Received 20 August 2016
Received in revised form 2 March 2017
Accepted 6 March 2017
Available online 7 March 2017

Keywords:
A. Amorphous materials
A. Halides
B. Intercalation reactions
C. Infrared spectroscopy
D. Electrochemical properties

ABSTRACT

The nacrite-NaCl nanohybrid material, $\mathbf{Si_2Al_2O_5(OH)_4}\cdot(1-(\boldsymbol{\alpha}+\boldsymbol{\delta}))$NaCl$\cdot(1-\boldsymbol{\delta})H_2O$ with $\{\boldsymbol{\alpha}=0.2, \boldsymbol{\delta}=0.02\}$, has been prepared at ambient temperature by straightforward intercalation of sodium chloride in the interlamellar space of Tunisian nacrite, a reference clay mineral. The structural identification of the elaborated nanohybrid has been determined by means of X-ray diffraction and infrared spectroscopy. Thermogravimetric analysis carried out that *in-situ* heat treatment of the elaborated nanohybrid induces an amorphous nanohybrid $\mathbf{Si_2Al_2O_7}\cdot(1-(\boldsymbol{\alpha}+\boldsymbol{\delta}))$NaCl at 723 K, proceeding with heating till 923 K leads to a highly amorphous and disordered nanohybrid material labeled $\mathbf{Si_2Al_2O_7}\cdot\{(1-(\boldsymbol{\alpha}+\boldsymbol{\delta}))/2\}Na_2O$. The electrochemical impedance spectroscopy reveals that the elaborated nanohybrid exhibits a fairly high ionic conductivity up to 10^{-2} S m^{-1} at higher temperatures and can be classified as a superionic conductor.

1. Introduction

Clay minerals are the most common components of all sediments and soils in the Earth's crust. Among a wide variety of clay resources, kaolin is considered as one of the most promising candidates due to its low cost, easy availability, nontoxicity, bulk properties and its surface chemical properties [1]. One side of the kaolinite layer is gibbsite-like with aluminium atoms octahedrally coordinated to corner oxygen atoms and hydroxyl groups. The other side of the layer constitutes a silica-like structure in which the silicon atoms are tetrahedrally coordinated to oxygen atoms. The adjacent layers are linked *via* hydrogen bonds (O—H···O) involving aluminol (Al—OH) and siloxane (Si—O) groups. As a consequence of this structure, the silica/oxygen and alumina/hydroxyl sheets are exposed and interact with different components in the soil [2]. Consequently, kaolin has potential environmental applications [3,4]. The kaolin group is divided in three polytypes (*i.e.* nacrite, kaolinite, dickite) in addition to halloysite their hydrated analogue [5].

Well-crystallized Tunisian nacrite was used in this work as a starting clay mineral economically viable and technically efficient [6]. This layered aluminosilicate material $\{Si_2Al_2O_5(OH)_4\}$contributes high chemical stability with a main basal distance d_{002} = 0.72 nm and has been previously characterized in the work of Ben Haj Amara and co-workers [6–9].

With such a configuration and by adding very low organic and/or inorganic precursor content to the layered silicate, it is possible to tailor nacrite and/or kaolin into various structures of nanohybrid materials [10–12]. However, hybridization is eventually accompanied by substantial modifications of the kaolin surface of this silicate layer due to the expansion of the interlamellar space and complexation *via* hydrogen bonding. The resultant nanohybrid materials combine the features of both the host clay mineral and the guest species. These nanohybrid materials have attracted much interest from researchers, since they frequently show unexpected and remarkable improvements in their physicochemical properties compared to the unmodified aluminosilicate mineral [13,14].

Indeed, three intercalation modes of alkali halides into the kaolin group have been distinguished: *Mode A* includes those species that are directly intercalated [15,16]. *Mode B* includes those species which can enter the interlayer space by means of an entraining agent such as hydrazine or ammonium acetate [16]. *Mode C* includes those species which can only be intercalated into the interlayer space by the displacement of a previously-intercalated compound such as dimethylsufoxide "DMSO" [16].

Otherwise, as well as Tunisian nacrite has been employed in the development of new nanohybrid materials with high functionalities and unique properties [8,9,17–22], it was possible to produce synthetic material labeled "metanacrite" on the basis of thermally

* Corresponding author.
E-mail address: nouhajaafar@yahoo.fr (N. Jaafar).

http://dx.doi.org/10.1016/j.materresbull.2017.03.011
0025-5408/

activated raw nacrite [21,23]. The calcination process may be presented by the following equation [21,23]:

$$\underset{\text{nacrite}}{Si_2Al_2O_5(OH)_4} \rightarrow \underset{\text{metanacrite}}{Si_2Al_2O_7} + \underset{\text{water}}{2H_2O}$$

Metanacrite possesses amorphous structure very different from the layered nacrite matrix with a disordered polymerized silicon/aluminium framework [21,23].

This paper presents a continuation of the existing bibliometric data focusing eventually on the intercalation of NaCl alkali halide in the interlayer space of kaolinite. The previous attempts of intercalations of NaCl into Tunisian nacrite material failed in the major experiments cases. However, by referring to the previous publications [16,24], sodium chloride has been intercalated into kaolinite from aqueous solutions based on the cited *mode C*, where ammonium acetate is used as an intermediate agent [24]. Moreover, a possible intercalation of a trace amount of NaCl alkali halide was reached by thermal solid state reaction based on *mode C via* displacement of a previously intercalated dimethylsulfoxid [16]. Indeed in the present work we succeed in the intercalation of NaCl within an ordered matrix, and the nacrite's layers were considered appropriate for our interest. In this regard, we followed an innovative and inexpensive protocol based on another intercalation mode with a different entraining agent and novel solutions to dissolve NaCl.

Based on this scenario, we found it interesting to investigate the behavior of nacrite-NaCl nanohybrid by means of X-ray diffraction (XRD), infrared spectroscopy (IR) and thermogravimetric analysis (TGA).The electrical/dielectric properties of this nanohybrid subjected to excitation of frequency under controlled temperature were studied. Finally, we demonstrated a correlation between structural and electrical properties opening new perspectives of application of this nanohybrid material in future device generations based on alkali elements.

2. Experimental details

2.1. Materials

2.1.1. Raw nacrite

Raw nacrite material used in this work as a starting material was collected from the mine of Jbel Slata located in the region of Kef in North Tunisia [6–9].

2.1.2. Hybridization of nacrite

In this study, *Mode B* was adopted, firstly, due to the strong interlayer bonds governed by van der Waals' forces between the hydrogen atoms of the hydroxyls in the octahedral sheet and the oxygen atoms in the tetrahedral sheet which prevent the direct incorporation of some substances into the nacrite interlamellar space [25]. Secondly, this process ensures the fast intercalation of the alkali halide without destruction of the nacrite framework compared to *Mode A*. Finally, the protocol of synthesis followed in *Mode B* is much easier in comparison to that in *Mode C*. For these reasons, potassium acetate "KAc" was the best entraining agent selected for the expansion of nacrite; KAc was widely utilized as a small and highly polar molecule for the synthesis of materials that cannot be directly intercalated [6,16]. The nacrite-KAc complex was obtained after 14 days of manipulation, where 51 g of potassium acetate (Normality = 26 N) were added to 4 g of raw nacrite and mechanically shaken [9]. The resulting nacrite-KAc complex was then washed two times with water and air dried leading to a stable-homogeneous hydrate [6,8], which constituted the starting material for the next step of the synthesis of the new hybrid material. Experiments based on the use of water as a solvent leads to incomplete intercalation of Na^+ cations. For this reason, different organic solvents (acetone, methanol, ethanol, glycerol and ethylene glycol) were tested until an intercalation of 0.82 g of NaCl (Prolabo) was achieved in presence of 20 ml of acetone (NaCl insoluble in acetone and sodium salts have poor solubility in comparison to lithium salts) at ambient temperature. After 9 days of mechanical shaking under a magnetic stirrer, the final product was obtained and labeled: nacrite-NaCl nanohybrid.

2.1.3. Elaboration of highly amorphous nanohybrid

The *in-situ* heat treatment of the elaborated nacrite-NaCl nanohybrid induces an amorphous nanohybrid at 723 K, proceeding with heating till 923 K leads to a highly amorphous and disordered nanohybrid material labeled: metanacrite-Na_2O nanohybrid.

2.2. Characterization set up

The hybridization of nacrite and the amorphization of the nanohybrid were controlled by means of X-ray diffraction, infrared spectroscopy, thermogravimetric analysis, electrochemical impedance spectroscopy.

X-ray diffraction (XRD) patterns were recorded at ambient temperature by reflection setting with a D8 Bruker installation monitored by the EVA-version Diffrac plus software (Bruker AXS GmbH, Karlsruhe, Germany) and using $CuK\alpha_1$ radiation (λ = 1.540598 Å) operating at 40 kV and 40 mA. Usual scanning parameters were 0.02°2θ as step size and 6 s as counting time per step over the angular range 5–55°2θ. The divergence slit, the two Soller slits, the antiscatter, and resolution slits were 0.5, 2.3, 2.3, 0.5, and 0.06°, respectively.

Infrared (IR) spectra were recorded at ambient temperature using a thermo scientific Nicolet IR 200 FT-IR with ATR Spectrometer, equipped with a diamond crystal and working in the medium IR wavenumber range [4000–400 cm^{-1}].

Thermogravimetric (TG) behavior was investigated from the ambient temperature up to 1073 K using a 92 SETARAM instrument in flowing air, along with a heating rate of 5° C/min.

Electrochemical impedance spectra (EIS) were obtained using a Hewlett-Packard (HP) 4192 analyzer. The impedance measurements were taken in an open circuit using two electrode configurations with signal amplitude of 50 mV and a frequency band ranging from 10 Hz to 13 MHz at different temperatures. The examined sample was pressed into pellet using a hydraulic press. To ensure good electrical contact between the sample and the electrical junctions, the pellet was sandwiched between two platinum electrodes to form a symmetrical cell. The cell was placed into a programmable oven coupled with a temperature controller from ambient to 923 K. The resulting data were fitted using the equivalent circuit of the *Z view* software.

3. Results and discussion

In the following sections, the crystallographic, vibrational, thermal characteristics as well as the electrical/dielectric behavior of the nacrite-NaCl nanohybrid material are detailed starting with X-ray diffraction analysis.

3.1. Modelling of X-ray diffraction pattern of nacrite-NaCl nanohybrid

Examining the experimental *XRD* pattern of the stable nacrite-NaCl nanohybrid in Fig. 1, a main 00*l* reflection with d_{002} = 1.10 nm basal spacing value can be seen. This increase is accompanied by the expansion of the interlayer space of nacrite along the c^* axis. This result is probably due to the incorporation of sodium chloride with one water sheet into the nacrite matrix.

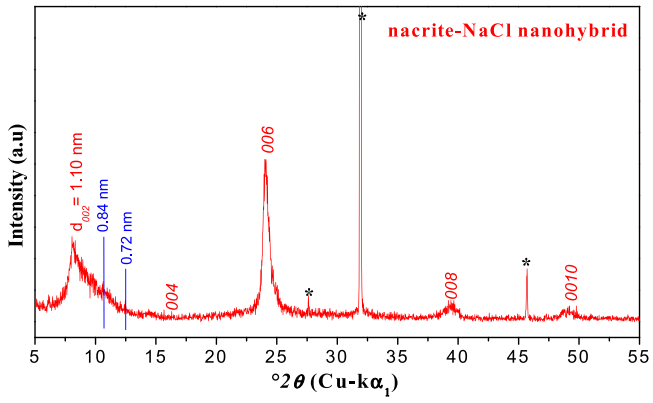

Fig. 1. Experimental XRD pattern of nacrite-NaCl nanohybrid material.
*: Reflections related to the excess of the salt: [Data Base PDF2: 01-070-2509. Compound name: Halite, syn.Formula NaCl].

The mean number of layers per crystallite, $\overline{M}$, deduced from the Debye-Scherrer formula:

$$\overline{M} = \frac{0.886\lambda}{l d_{00l}.FWHM(^{\circ}2\theta).\cos\theta_{00l}} \quad (1)$$

where λ is the wavelength used, *FWHM* ($^{\circ}2\theta$) represents the angular width at half-height of *00l* XRD reflection and (l d $_{00l}$) the apparent distance deduced from the maximum intensity for all measurable reflections over the *5–55°2θ* angular range. $\overline{M}$ decreases from "70 ± 1" of raw nacrite [8] to "12 ± 1" of nacrite-NaCl nanohybrid. This result can be interpreted as particle cleavage and as a break of coherence during the intercalation process.

Concerning, the coefficient of variation introduced by Bailey [26].

$$CV = \frac{100}{d_m}\left[\frac{\sum (d_n - d_m)^2}{n-1}\right]^{1/2} \quad (2)$$

where d_n, d_m and n represent the apparent spacing determined from the maximum intensity for all measurable reflections (l d $_{00l}$), the mean basal distance and the number of *00l* reflections respectively. For a regular system, the *CV* coefficient is less than 0.75 indicating a homogenous complex.

The value of the coefficient of variation *CV* (Eq. (2)) and the rationality of *00l* the basal reflections (Table 1) in the case of nacrite-NaCl nanohybrid suggest a homogenous sample character. However, the high value of the full width at half maximum *FWHM* of the mean reflection at around (1.111°2θ) (Table 1) is interpreted as a contradictory result. This is highlighted by the fact that the *FWHM* could be significantly affected by stress, strain and interstratifications. Additional reflections are attributed to excess of salt and are marked with (*).

The quantitative study will now be considered because it is much more convincing than the qualitative one. For these reasons, a modelling computer program designed to perform calculations of diffracted intensities was used.

The overall fit quality is assessed using the unweighted *Rp* parameter [27]:

$$Rp = \sqrt{\frac{\sum \left[\mathrm{I}(2\theta_i)_{obs} - \mathrm{I}(2\theta_i)_{calc}\right]^2}{\sqrt{\left[\mathrm{I}(2\theta_i)_{obs}\right]^2}}} \quad (3)$$

where, I_{obs} and I_{calc} represent measured and calculated intensities, respectively, at the $2\theta_i$ position, the subscript i running over all points in the refined angular range. *Rp* is mainly influenced by the most intense diffraction maxima, such as the *00l* reflections, which contains essential information on the proportions of the different layer types and layer thickness.

The theoretical XRD pattern related to the nacrite-NaCl specimen was reproduced to fit the experimental one. The best model belongs to the lowest reliability factor (7.14%). Furthermore, we observe a satisfactory agreement between the experimental and theoretical XRD patterns according to both intensity and profile (Fig. 2).

Finally, we deduce the structural parameters of the stable nacrite-NaCl nanohybrid per half unit-cell:

- One Na^+ cation located at $z = 0.98 \pm 0.01$ nm
- One Cl^- anion located at $z = 0.66 \pm 0.01$ nm
- One water molecule placed at $z = 0.75 \pm 0.01$ nm and is sandwiched between the cation and the anion.

z coordinates are taken from the oxygen surface oxygen along the normal to the layer.

This model suggests the presence of a hydrated salt and is in concordance with the qualitative analysis.

To sum up, the intercalated species stand vertically in the interlamellar space of nacrite, where the cations are located close to the ditrigonal holes of the tetrahedral layers and the anions are located close to the inner-surface hydroxyls of the octahedral layer of the subsequent sheet (Scheme 1).

The quantitative study of the nacrite-NaCl nanohybrid clearly showed an interstratified stacking mode characterized by a segregation tendency consisting of a total demixion of three types of layers:

- Layer *A* at 1.10 nm attributed to a major fraction (78%) of the intercalated nacrite.
- Layer *B* at 0.84 nm related to a minor fraction (20%) of the hydrate.
- Layer *C* at 0.72 nm related to a minor fraction (2%) of the unexpanded clay.

The proportions of each layer {$W_A = 0.78$, $W_B = 0.20$, $W_C = 0.02$}.
The conditional probability of passing from layer i to layer j (P_{ij}): {$P_{AA} = 1$, $P_{AB} = 0$, $P_{AC} = 0$, $P_{BA} = 0$, $P_{BB} = 1$, $P_{BC} = 0$, $P_{CA} = 0$, $P_{CB} = 0$, $P_{CC} = 1$}.
The mean number of layers per stacking within each crystallite equals 14 ± 1, this value is very close to the experimental value $\overline{M}$ obtained from the qualitative analysis.
The structural formula per half unit cell of the studied nanohybrid at ambient temperature was then determined as;

Table 1
Principal qualitative XRD results of nacrite-NaCl nanohybrid.

nanohybrid	*nacrite –NaCl*				
00l reflections	*002*	*004*	*006*	*008*	*0010*
(l.d $_{00l}$) (nm)	1.100	1.110	1.099	1.094	1.096
The full width at half maximum:*FWHM* ($^{\circ}2\theta$)	1.111	0.847	0.494	0.576	0.651
The mean number of layers per crystallite:$\overline{M}$			12		
The coefficient of variation: *CV*			0.56 < 0.75		

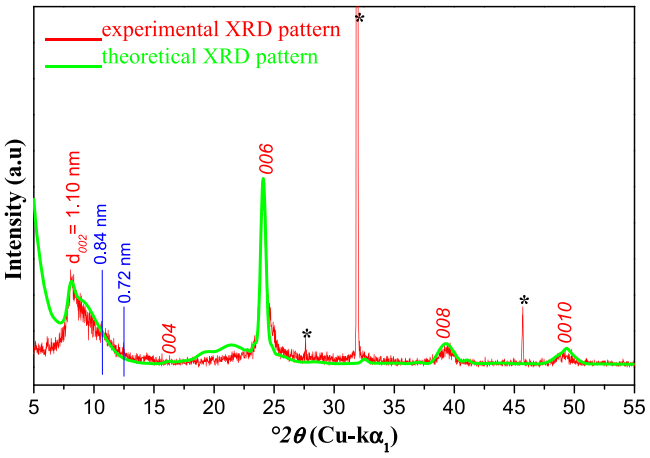

Fig. 2. Best agreement between experimental and theoretical XRD profiles of nacrite-NaCl nanohybrid material.

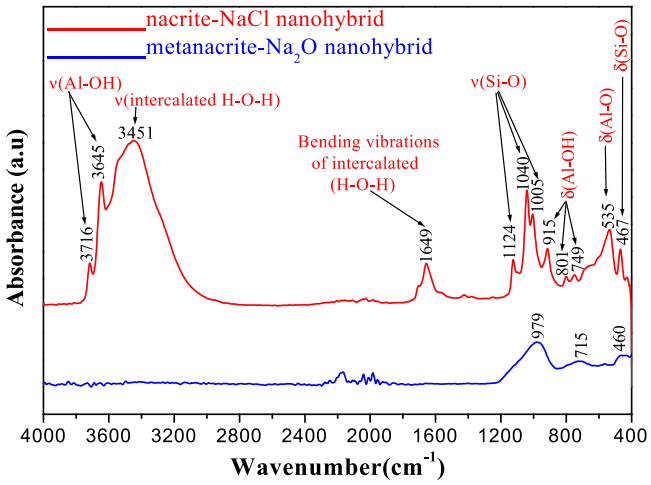

Fig. 3. Wavenumbers and assignments of the IR absorption bands in the 4000–400 cm^{-1} spectral region for nacrite-NaCl nanohybrid and metanacrite-Na_2O nanohybrid.

$$\mathbf{(1-(\alpha+\delta))\ \{Si_2Al_2O_5(OH)_4\cdot NaCl\cdot 1H_2O\} + \alpha\ \{Si_2Al_2O_5(OH)_4\cdot 1H_2O\} + \delta\ \{Si_2Al_2O_5(OH)_4\cdot 1H_2O\} = Si_2Al_2O_5(OH)_4\cdot(1-(\alpha+\delta))NaCl\cdot(1-\delta)H_2O}$$

with $\alpha = 0.2$ (the fraction of the hydrate of nacrite) and $\delta = 0.02$ (the fraction of non intercalated nacrite).

3.2. IR spectroscopy of nacrite-NaCl nanohybrid

By comparing the spectrum of nacrite-NaCl nanohybrid (Fig. 3) to the spectrum of the untreated nacrite [19], it is possible to follow the modification of the stretching and deformation vibrations. These changes are manifested in the recorded spectrum of the nacrite-NaCl nanohybrid by:

i) The weakening of the OH lattice stretching band since it is located in the envelope of the strong HOH band.

ii) The appearance of HOH stretching and bending vibrations which do not occur in the spectrum of raw nacrite.

iii) Shifts of δ(Al—OH) and δ(Al—O) deformation vibrations to lower frequencies.

iv) Shifts of the Si—O stretching ν(Si—O) and deformation δ(Si—O) vibrations to lower frequencies.

The weakening of the ν(Al—OH) stretching vibrations as well as the shifts of the δ(Al—OH) deformation vibrations, indicate that the inner surface hydroxyls of the octahedral layer form hydrogen bonds with the Cl^- ions: ***O—H···Cl***$^-$. It is important to note that the hydrogen bonds between the chlorides and the inner surface OH groups are much stronger than those between the chlorides and the inner OH groups [10].

A concomitant appearance of a new and strong water band at 3451 cm^{-1} is an indication that the intercalated H_2O molecule is bonded to both ions of the salt, the alkali and the halide [15,28]. The sodium cation is bound to the H_2O oxygen by an ion-dipole electrostatic interaction whereas the chloride anion is bound through a hydrogen bond in which the water molecule acts as a proton donor as follows: ***Na···O(H)—H···Cl*** [15,28].

It should be mentioned that shifts of the SiO stretching and deformation vibrations in the infrared spectrum of the studied nanohybrid indicate that these bonds are weak. This is due to the strength of the bonds formed between water molecules and Cl^- ions. Consequently, the ability of the inserted water molecule to donate its second proton to an oxygen atom of the silicate layer leads to a weak ***Si—O···H—OH*** hydrogen bond. This result is in great accordance with the previous studies of Yariv et al. [10] about the keying of chloride salts into the kaolin-type minerals.

Finally, IR spectroscopy proved that:

- The Cl^- halide anion interacts with the inner surface hydroxyls of the alumina sheet through hydrogen-bonding.
- The Na^+ alkali cation interacts electrostatically with the negatively charged oxygens of the inner-surface oxygen of the silica sheet.
- The intercalated water molecule only interacts with the Cl^- and Na^+ ions.

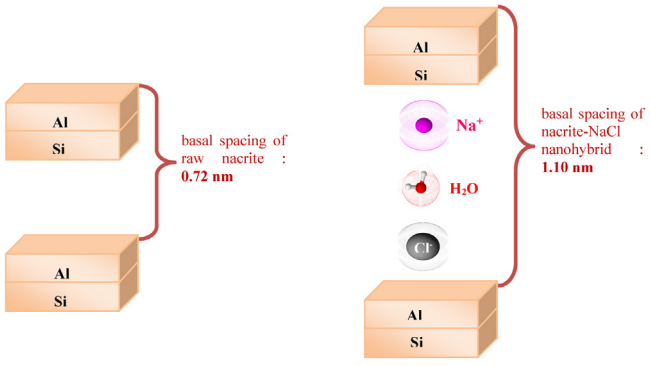

Scheme 1. (a) Schematic representation of the alumina and silica-like layers of raw nacrite; (b) Schematic representation of the nacrite-NaCl nanohybrid.

3.3. Evolution of ATG from nacrite-NaCl nanohybrid to metanacrite-Na_2O nanohybrid

The thermal analysis of the nacrite-NaCl nanohybrid $\mathbf{Si_2Al_2O_5(OH)_4\cdot(1-(\alpha+\delta))NaCl\cdot(1-\delta)H_2O}$ with $\{\alpha = 0.2,\ \delta = 0.02,\ \mathbf{(1-(\alpha+\delta))} = 0.78$ and $\mathbf{(1-\delta)} = 0.98\}$ indicates that *in-situ* heat treatment induces an amorphous nanohybrid at 723 K, proceeding with heating till 873 K leads to a highly amorphous and disordered nanohybrid material.

Thermogravimetric curves give evidence that the nanohybrid nacrite-NaCl gradually loses mass from 298 to 1073 K (Fig. 4, Table 2).

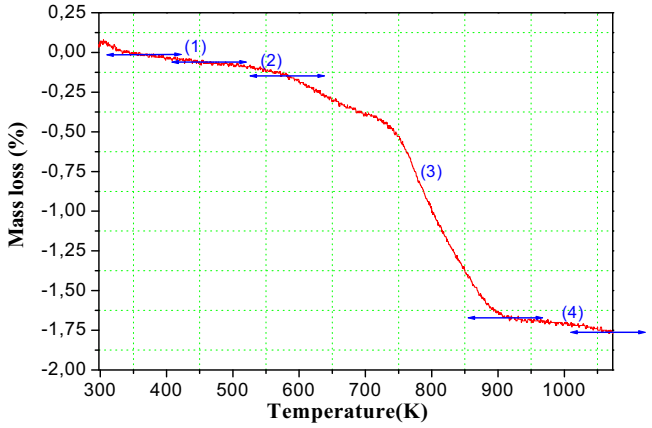

Fig. 4. The TG curves of the nacrite-NaCl nanohybrid heated from 298 to 1073 K.

Table 2
Mass loss of the elaborated nacrite-NaCl nanohybrid.

	$\frac{\Delta m}{m}$	–n H_2O *per half unit-cell*
mass loss 1	1.14%	$-1H_2O$
mass loss 2	0.49%	$-1H_2O$
mass loss 3	12.78%	$-2H_2O$
mass loss 4	0.60%	$-1H_2O$
Total mass loss	15.41%	

- The first remarkable mass loss is observed between 298 and 423 K corresponds to the removal of water molecules in the pores.
- A second mass loss (0.49%) occured between 423 and 623 K and belongs to the removal of the intercalated water molecule and confirms the results obtained by XRD of nacrite-NaCl nanohybrid.
- The third mass loss is centered between 723 and 923 K (12.78%) and was due to the calcination process of nacrite-NaCl nanohybrid. This loss confirms the departure of structural water. *At T = 723* K, the chemical decomposition of the nanohybrid per half-unit cell can be expressed as follows:

$$\mathbf{Si_2Al_2O_5(OH)_4}\cdot(1-(\boldsymbol{\alpha}+\boldsymbol{\delta}))\mathrm{NaCl} \rightarrow \mathbf{Si_2Al_2O_7}\cdot(1-(\boldsymbol{\alpha}+\boldsymbol{\delta}))\mathrm{NaCl} + 2H_2O.$$

The product formed during the calcination is labeled amorphous nanohybrid: $\mathbf{Si_2Al_2O_7}\cdot(1-(\boldsymbol{\alpha}+\boldsymbol{\delta}))\mathrm{NaCl}$ (Table 3).

At $T \geq 723$ K, this step is eventually accompanied by the evolution of the hydrogen halide which results from the following thermal hydrolysis [29,30]:

$$\mathbf{Si_2Al_2O_7} + (\mathbf{1}-(\boldsymbol{\alpha}+\boldsymbol{\delta}))\mathbf{NaCl} \rightarrow \mathbf{Si_2Al_2O_7}\cdot\frac{(\mathbf{1}-(\boldsymbol{\alpha}+\boldsymbol{\delta}))}{\mathbf{2}}\mathbf{Na_2O} + (\mathbf{1}-(\boldsymbol{\alpha}+\boldsymbol{\delta}))\mathbf{HCl} - \frac{(\mathbf{1}-(\boldsymbol{\alpha}+\boldsymbol{\delta}))}{\mathbf{2}}\mathbf{H_2O}.$$

During the calcination process, a liberated water molecule from the clay surface is associated with Cl^- to form volatile HCl. The volatilization of HCl is responsible for a significant amount of thermal mass loss of the examined nanohybrid. This phenomenon causes the trapping of Na_2O sodium oxide within the metanacrite matrix. The nanohybrid formed during this step is highly amorphous and has the following chemical formula: $\mathbf{Si_2Al_2O_7}\cdot\{(\mathbf{1}-(\boldsymbol{\alpha}+\boldsymbol{\delta}))/\mathbf{2}\}\mathbf{Na_2O}$ (Table 3).

- A fourth mass loss occurred between 873 and 1073 K may be due to the evolution of hygroscopic water belonging to the sphere of hydration of Na^+ cation.

To confirm the newly developed highly amorphous phase of $\mathbf{Si_2Al_2O_7}\cdot\{(1-(\boldsymbol{\alpha}+\boldsymbol{\delta}))/2\}Na_2O$, *ex-situ* infrared spectroscopy (IR) analysis is carried out. As shown in Fig. 3, it is possible to follow the modifications of the stretching and deformation vibrations by comparing the IR spectra of metanacrite-Na_2O and nacrite-NaCl nanohybrids. Indeed, at high wavenumbers, it should be mentioned that no bands are detected in the infrared spectrum of metanacrite-Na_2O, indicating the disappearance of the OH lattice stretching band and lose of structural and intercalated water during heat-treatment. However, at low wavenumbers, the stretching vibrations ν(Si—O) located at 1005, 1040, 1124 cm^{-1} and the Si—O deformation vibrations δ(Si—O) located at 469 cm^{-1} are evidently observed with a slight change in their shape and intensity, while the δ(Al—O) deformation vibrations are shifted to high wavenumbers from 535 to 715 cm^{-1} and the δ(Al—OH) deformation vibrations placed at 749, 801 and 915 cm^{-1} in the spectrum of nacrite-NaCl are omitted in the spectrum of metanacrite-Na_2O. All these changes in the infrared spectrum between metanacrite-Na_2O and nacrite-NaCl imply that layered structure is then destroyed and transformed into a disordered metastate.

In the other hand, the similarity between the IR spectra of metanacrite-Na_2O and metanacrite [23] confirms the amorphocity behavior of the metanacrite-Na_2O nanohybrid. Nevertheless, we note a slight shift and shape deformation between them indicating the presence of content of sodium oxide trapped into the metanacrite framework which corroborate the XRD and TG analysis of this highly amorphous nanohybrid.

3.4. Electrochemical impedance spectroscopy of nacrite-NaCl nanohybrid subjected to excitation of frequency under controlled temperature

3.4.1. Nyquist diagrams

Nyquist diagrams illustrate the existence of semicircles in the complex plane (Fig. 5). At high temperature, these semi-arcs shift towards higher frequencies with a significant reduction of their size from 573 to 923 K. We point out, that nacrite-NaCl nanohybrid becomes more conductive at high temperature. We think that this phenomenon is attributed to the deformation and destruction of some physical characteristics of the host clay framework and to some chemical characteristics of NaCl alkali halide. The resulting data were fitted using the *Zview* software. The best electrical circuit which reflects the response of the sample nacrite-NaCl is an equivalent circuit type: R_s//(CPE, R_p). R_s represents the resistance of

Table 3
Phase transformations during *in-situ* heat-treatement of nacrite-NaCl nanohybrid from ambient temperature to 873 K.

Temperature	Nanohybrid	Chemical formula ($\boldsymbol{\alpha}$ = 0.2, $\boldsymbol{\delta}$ = 0.02)	Phase
T = 298 K	nacrite-NaCl	$Si_2Al_2O_5(OH)_4\cdot(1-(\alpha+\delta))NaCl\cdot(1-\delta)H_2O$	crystalline
T = 723 K	metanacrite-NaCl	$Si_2Al_2O_7\cdot(1-(\alpha+\delta))NaCl$	amorphous
T = 873 K	metanacrite-Na_2O	$Si_2Al_2O_7\cdot\{(1-(\alpha+\delta))/2\}Na_2O$	highly amorphous

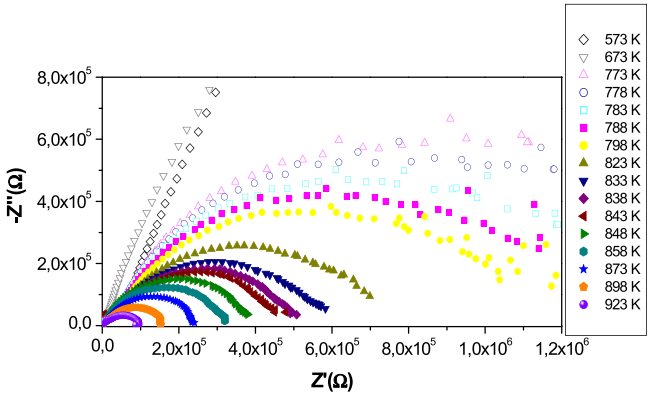

Fig. 5. Complex impedance diagrams of nacrite-NaCl nanohybrid over the temperature range (573–923 K).

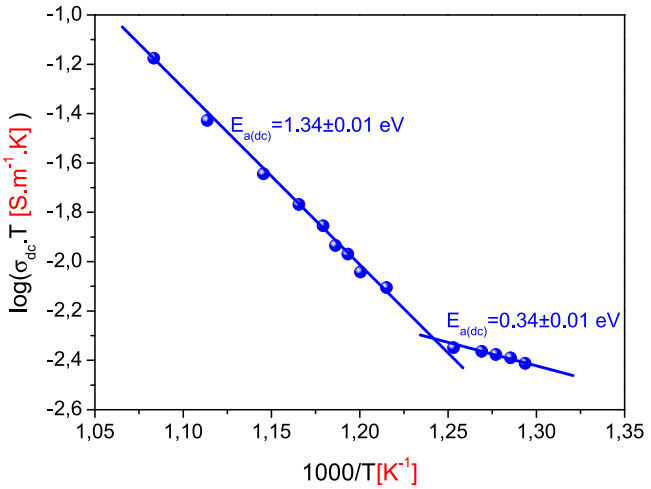

Fig. 6. $\log(\sigma_{dc}\cdot T) = f(1000/T)$ of nacrite-NaCl nanohybrid material in the temperature range between 773–923 K.

grain connected in series, R is the resistance of grain connected in parallel to a constant phase angle capability (CPE).

3.4.2. AC and DC electrical conductivity

The *dc* conductivity of nacrite-NaCl nanohybrid increases from ($5.01.10^{-6}$ S m^{-1}) at 773 K up to ($7.24.10^{-5}$ S m^{-1}) at 923 K (Table 4). The logarithmic variation of the *dc* conductivity shows two slopes, which corresponds to the activation energies. These values suggest an ionic conduction process (Fig. 6). Moreover, the break in the curve, attributed to the phase transition from crystalline to amorphous state as determined in thermal analysis, indicates that the ionic conductivity is strongly enhanced by the amorphization of the nanohybrid.

The values of the activation energies $E_{a(ac)}$ were determined from the log curve log (σ_{ac}) vs (1000/T) (Fig. 6, Table 5). Measurements of ac conductivity at high frequency (10 MHz) indicates that the conductivity σ_{ac} increases in terms of temperature from ($3.63.10^{-3}$ S m^{-1}) at 773 K up to ($3.01.10^{-2}$ S m^{-1}) at 923 K (Table 4). The increase of *ac* conductivity measured at high frequencies (10 MHz) is related to that of the number of free sodium cations in the nanohybrid matrix and designates that the ionic transport mechanism can be interpreted by the thermally activated hopping process.

In the next part we detail the charge carriers responsible for conduction in our nanohybrid before and after the temperature of calcination.

- *Before calcination*, the nacrite-NaCl nanohybrid has a highly crystalline structure according to the XRD profile. Based on the strong interactions between the silicate network and the intercalated species determined by IR, the structure of the aluminosilicate ion (O^{2-}, OH^- and H^+) can not contribute to the conduction in the nanohybrid.
- In addition, H^+ and OH^- ions of water molecules intercalated are eliminated due to dehydration that starts from 373 K as shown by TGA. On the other hand, Na^+ is known as an excellent charge carrier in superionic solids motivated by its small ionic radius, its low atomic mass. Besides Cl^- anion appears to be a bit less mobile than the Na^+ cation. In conclusion, Na^+ is the dominant charge carrier in the nacrite-NaCl nanohybrid.
- *During calcination*, in the temperature range between 723 and 923 K, the nacrite-NaCl nanohybrid becomes metanacrite-NaCl nanohybrid then metanacrite-Na_2O nanohybrid containing large

Table 5
ac activation energies values from 773 to 923 K of nacrite-NaCl nanohybrid material.

Frequencies	*ac* activation energies: $E_{a(ac)}$ [eV]	
	Temperature range 773 → 798 K	Temperature range 798 → 923 K
100 Hz	0.29	1.22
1 MHz	0.16	0.40
5 MHz	0.39	0.47
10 MHz	1.15	0.95

Table 4
ac and *dc* conductivity values of nacrite-NaCl nanohybrid.

Temperature [K]	*ac* conductivity: σ_{dc} (S.m^{-1})	*dc* conductivity: σ_{ac} (S m^{-1})			
		f = 100 Hz	*f* = 1 MHz	*f* = 5 MHz	*f* = 10 MHz
773	$5.01.10^{-6}$	$5.01.10^{-6}$	$1.51.10^{-4}$	$3.23.10^{-4}$	$3.63.10^{-3}$
778	$5.24.10^{-6}$	$5.24.10^{-6}$	$1.51.10^{-4}$	$3.38.10^{-4}$	$4.07.10^{-3}$
783	$5.37.10^{-6}$	$5.37.10^{-6}$	$1.54.10^{-4}$	$3.46.10^{-4}$	$6.16.10^{-3}$
788	$5.49.10^{-6}$	$5.49.10^{-6}$	$1.54.10^{-4}$	$3.63.10^{-4}$	$6.45.10^{-3}$
798	$5.62.10^{-6}$	$5.62.10^{-6}$	$1.58.10^{-4}$	$3.89.10^{-4}$	$6.60.10^{-3}$
823	$9.54.10^{-6}$	$9.54.10^{-6}$	$1.62.10^{-4}$	$4.07.10^{-4}$	$6.76.10^{-3}$
833	$1.09.10^{-5}$	$1.12.10^{-5}$	$1.69.10^{-4}$	$4.26.10^{-4}$	$6.91.10^{-3}$
838	$1.28.10^{-5}$	$1.28.10^{-5}$	$1.73.10^{-4}$	$4.26.10^{-4}$	$7.58.10^{-3}$
843	$1.38.10^{-5}$	$1.38.10^{-5}$	$1.77.10^{-4}$	$4.36.10^{-4}$	$8.31.10^{-3}$
848	$1.65.10^{-5}$	$1.65.10^{-5}$	$2.13.10^{-4}$	$5.37.10^{-4}$	$1.00.10^{-2}$
858	$1.99.10^{-5}$	$1.94.10^{-5}$	$2.29.10^{-4}$	$5.88.10^{-4}$	$1.00.10^{-2}$
873	$2.60.10^{-5}$	$2.63.10^{-5}$	$2.51.10^{-4}$	$6.76.10^{-4}$	$1.02.10^{-2}$
898	$4.16.10^{-5}$	$4.07.10^{-5}$	$2.95.10^{-4}$	$8.12.10^{-4}$	$1.17.10^{-2}$
923	$7.24.10^{-5}$	$7.24.10^{-5}$	$3.09.10^{-4}$	$8.12.10^{-4}$	$3.01.10^{-2}$

amount of amorphous aluminosilicate (Table 3). TGA indicated that in this temperature range, the de-hydroxylation is characterized by the elimination of inner-surface hydroxyls and inner hydroxyl of nacrite framework. Therefore, OH^- and H^+ do not contribute to ion conduction process. In addition, a new Si—O—Al is created, which prevents O^{2-} anions to participate into the ionic transport mechanism.

Hence, concerning the amorphous nanohybrid $\mathbf{Si_2Al_2O_7}\cdot(1-(\boldsymbol{\alpha}+\boldsymbol{\delta}))$NaCl (Table 4), the corresponding ionic conductivity increases significantly in terms of temperature. The amorphous structure favors the motion of Na^+ ions. In addition, the highly amorphous nanohybrid $\mathbf{Si_2Al_2O_7}\cdot\{(1-(\boldsymbol{\alpha}+\boldsymbol{\delta}))/2\}Na_2O$ showed a higher conductivity value. This improvement in conductivity may be explained by the presence of sodium content oxide into the highly amorphous nanohybrid matrix through which the mobile ions migrate. Different models have been proposed to describe the appropriate *dc* conduction mechanism for this elaborated highly amorphous nanohybrid. **The 1st model**: **The NBO-BO switching model** [31–35] suggests that ion transport occurs during the exchange process between the "Non-Bridging oxygens NBO" and "Bridging oxygens BO". This process causes the destabilization of the cations (alkali ions) and requires a small activation barrier. **The 2nd model**: **The alkali ion transport model** proposed by Anderson and Stuart [36]. It considers that the alkali oxide (sodium oxide) reacted completely with the network by creating oxygen non-bridging and free alkali ions (Na^+). The model treats all alkali ions as effective charge carriers. The alkali ion moves to a position equivalent to another by crossing a characteristic migration barrier, this model requires $E_{a(dc)} \sim 1$ eV. We conclude then that the model "NBO-BO switching" is not consistent with the experimental results. However, the alkali ion transport model proposed by Anderson and Stuart is the best model that adequately reflects the *dc* conduction mechanism (Fig. 6 and Table 6). We conclude that the Na^+ cation is the predominant charge carrier for the highly disordered nanohybrid.

According to these experimental results, we conclude that the amorphous structure facilitates the motion of ions compared to that in the crystalline state. We conclude that the disorder and defects are responsible for the motion of charge carriers. To conclude, the ordered nanohybrid "nacrite-NaCl" behaves like a good ionic conductor motivated by mobility and low ionic radius of Na^+ cation incorporated into the nanohybrid matrix. The highly disordered nanohybrid "metanacrite-Na_2O" exhibits a higher conductivity and behaves like a superionic conductor due to the competition of the size of the alkali metal ion Na^+ and the presence of disorder and defects. This suggests that there is a close correlation between the structure and conductivity.

Finally, we compare our experimental results with a popular class of electrolytes from the literature possessing high ionic conductivity based on glassy amorphous alkali metal phosphates

Table 6
Assessment of the activation energies for dc conductivity of our elaborated amorphous clay nanohybrid with a serie of composite materials based on glassy phosphate.

Class of materials	Ionic conductor materials	$E_{a(dc)}$ (eV)	References
Clay minerals	$Si_2Al_2O_7\cdot\{(1-(\alpha+\delta))/2\}Na_2O$	1.34	this work
Glassy phosphates	$LiLa(PO_3)_4$	0.40	[38]
	$LiDy(PO_3)_4$	0.96	[39]
	$LiGd(PO_3)_4$	0.96 and 1.7	[40]
	$AgLa(PO_3)_4$	1.22	[40]
	$KY(PO_3)_4$	1.43	[41]
	$LiK(PO_3)_2$	1.89	[42]
	$NaCeP_2O_7$	1.39	[43]

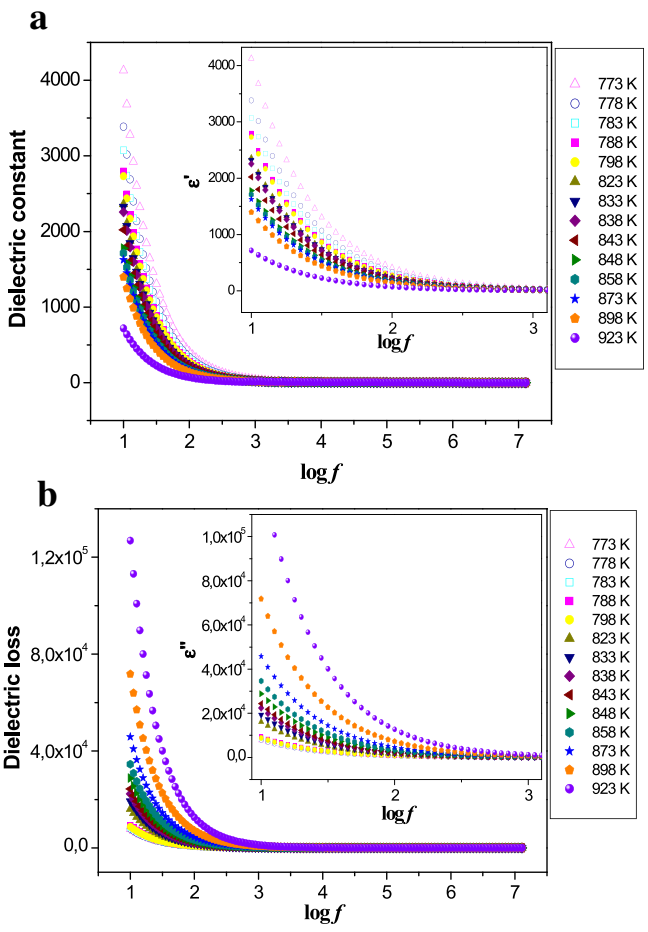

Fig. 7. a. $\varepsilon' = f(\log f)$ of nacrite-NaCl nanohybrid from 773 to 923 K. b. $\varepsilon'' = f(\log f)$ nacrite-NaCl nanohybrid from 773 to 923 K.

[37]. We deduce the sensitivity of the ionic conduction to the guest species and physical properties composition of the host matrix (see Table 6).

3.4.3. Dielectric permittivity

Moreover, we discover that: At low frequencies (Fig. 7a and b), the decrease in the dielectric constant and the increase of the dielectric loss in terms of temperature corroborates the *ac* measurements. This result confirms also the thermal behavior of the studied nanohybrid characterized by the destruction of the ordered structure of the nanohybrid in function of temperature that does not allow the isolation of the Na^+ cation in a localized site, and therefore a faster motion of sodium cations may be expected.

Another interesting observation is that at a higher frequency ($f > 1$ kHz) and for all temperatures (Fig. 7a and b), the variation of dielectric functions (ε' and ε'') slows down and becomes almost constant. This behavior may be accredited to the fact that as the frequency increases, the overall polarization (electronic, orientation, space charge polarizations, etc.) decreases and the dielectric functions become almost frequency independent.

4. Conclusions

Summarizing, new nanohybrid material, namely nacrite host matrix intercalated with NaCl alkali halide salt has been prepared and characterized by several techniques. The increase of the host matrix interlamellar distance from 0.72 up to 1.10 nm shows a successful intercalation of the guest molecule maintaining, in the

same time, the layered structure. The intercalation process was also verified by accurate infrared spectroscopy. Additionally, the electrical/dielectric properties were successfully enhanced by heating to 923 K, showing that the thermal treatment employed in this work is an effective route to obtain an amorphous nanohybrid material with original properties.

References

[1] M. Castellano, A. Turturro, P. Riani, T. Montanari, E. Finocchio, G. Ramis, G. Busca, Bulk and surface properties of commercial kaolins, Appl. Clay. Sci. 48 (2010) 446–454.
[2] F. Wypych, K.G. Satyanarayana, Clay Surfaces, Fundamentals and Applications, Academic Press/Elsevier, Waltham/Amsterdam, 2004.
[3] W. Rondón, D. Freire, Z. de Benzo, A.B. Sifontes, Y. González, M. Valero, J.L. Brito, Application of 3A zeolite prepared from venezuelan kaolin for removal of Pb(II) from wastewater and its determination by flame atomic absorption spectrometry, Am. J. Anal. Chem. 4 (2013) 584–594.
[4] P. Kabwadza-Corner, M.W. Munthali, E. Johan, N. Matsue, Comparative study of copper adsorptivity and selectivity toward zeolites, Am. J. Anal. Chem. 5 (2014) 395–405.
[5] M.F. Brigatti, E. Galan, B.K.G. Theng, Structure and Mineralogy of Clay Minerals. Handbook of Clay Science: Developments Clay Science, Vol. 5, Part A: Fundamentals, 2nd ed., Elsevier, Amsterdam, 2013.
[6] A. Ben Haj Amara, X-ray diffraction, infrared and TGA/DTG analysis of hydrated nacrite, Clay Miner. 32 (1997) 463–470.
[7] A. Ben Haj Amara, J. Ben Brahim, A. Plançon, H. Ben Rhaiem, G. Besson, Etude structurale d'une nacrite tunisienne, J. Appl. Crystallogr. 30 (1997) 338–344.
[8] A. Ben Haj Amara, A. Plançon, J. Ben Brahim, H. Ben Rhaiem, XRD Study of the stacking mode in natural and hydrated nacrite, Mater. Sci. Forum 278–81 (1998) 809–813.
[9] A. Ben Haj Amara, H. Ben Rhaiem, A. Plançon, Structural evolution of nacrite as a function of the nature of the intercalated organic molecules, J. Appl. Crystallogr. 33 (2000) 1351–1359.
[10] S. Yariv, I. Lapides, K.H. Michaelian, N. Lahav, Thermal intercalation of alkali halides into kaolinite, J. Therm. Anal. Calorim. 56 (1999) 865–884.
[11] K. Orzechowski, T. Slonka, J. Glowinski, Dielectric properties of intercalated kaolinite, J. Phys. Chem. Solids 67 (2006) 915–919.
[12] S. Letaief, T. Diaco, W. Pell, S.I. Gorelsky, C. Detellier, Ionic conductivity of nanostructured hybrid materials designed from imidazolium ionic liquids and kaolinite, Chem. Mater. 20 (2008) 7136–7142.
[13] K.H. Michaelian, I. Lapides, N. Lahav, S. Yariv, I. Brodsky, Infrared study of the intercalation of kaolinite by caesium bromide and caesium iodide, J. Colloid Interface Sci. 204 (1998) 389–393.
[14] V. Vagvolgyi, J. Kovacs, E. Horvath, J. Kristof, E. Mako, Investigation of mechanochemically modified kaolinite surfaces by thermoanalytical and spectroscopic methods, J. Colloid Interface Sci. 317 (2008) 523–529.
[15] K.H. Michaelian, S. Yariv, A. Nasser, Study of the interactions between caesium bromide and kaolinite by photoacoustic and diffuse reflectance infrared spectroscopy, Can. J. Chem. 69 (1991) 749–754.
[16] I. Lapides, N. Lahav, K.H. Michaelian, S. Yariv, X-Ray study of the thermal intercalation of alkali halides into kaolinite, J. Therm. Anal. 49 (1997) 1423–1432.
[17] N. Jaafar, H. Ben Rhaiem, A. Ben Haj Amara, Synthesis, characterization and applications of a new nanohybrid composite: nacrite/$MgCl_2.6H_2O$/ethanol, international conference on composite materials & renewable energy applications (ICCMREA), IEEE Xplore Digit. Lib. (2014) 1–6.
[18] N. Jaafar, S. Naamen, H. Ben Rhaiem, A. Ben Haj Amara, Elaboration of amorphous-clay hybrid: ($Al_2Si_2O_7$. Li_2O) designed as a single ion conducting solid electrolyte for Li-ion batteries, Am. J. Anal. Chem. 5 (2014) 1261–1272.
[19] N. Jaafar, S. Naamen, H. Ben Rhaiem, A. Ben Haj Amara, Functionalization and structural characterization of a novel nacrite-LiCl nanohybrid material, Am. J. Anal. Chem. 6 (2015) 202–215 (Special Issue on X-Ray Diffraction.
[20] S. Naamen, N. Jaafar, H. Ben Rhaiem, A. Ben Haj Amara, A. Plançon, F. Muller, XRD investigation of the intercalation of nacrite with cesium chloride, Clay Miner. 51 (1) (2016) 29–38.
[21] N. Jaafar, H. Ben Rhaiem, A. Ben Haj Amara, in: Dr. Gustavo Morari Do Nascimento (Ed.), Structural and Electrochemical Properties of Cementitious and Hybrid Materials Based on Nacrite, Clays, Clay Minerals and Ceramic Materials Based on Clay Minerals, 9, InTech, 2016, doi:http://dx.doi.org/10.5772/61594.
[22] N. Jaafar, H. Ben Rhaiem, A. Ben Haj Amara, Crystallographic vibrational, thermal and electrochemical properties of nacrite-NH_4Cl nanohybrid, Appl. Clay Sci. 132–133 (2016) 600–610.
[23] N. Jaafar, H. Ben Rhaiem, A. Ben Haj Amara, Correlation between electrochemical impedance spectroscopy and structural properties of amorphous tunisian metanacrite synthetic material, Adv. Mater. Sci. Eng. (2014) 1–10.
[24] A. Weiss, W. Thielepape, W. Ritter, H. Schaefer, Israel Universities Press, Proc. Intern. Clay. Conf., Jerusalem, 11966, pp. 277.
[25] M. Cruz, H. Jacobs, J.J. Fripiat, Interlayer Bonding in Kaolin Minerals, Proceedings of the International Clay Conference, 1972, CSIC, Madrid: Division de Ciencias, Madrid, Spain, 1973, pp. 35–46.
[26] S.W. Bailey, Nomenclature for regular interstratifications, Clay Miner. 17 (1982) 243–248.
[27] S.A. Howard, K.D. Preston, Profile fitting of powder diffraction patterns, in: D.L. Bish, J.E. Post (Eds.), Modern Powder Diffraction: Reviews in Mineralogy, Mineralogical Society of America, Washington DC, 1989, pp. 217–275.
[28] R.L. Frost, J. Kristof, E. Mako, J.T. Kloprogge, Modification of the hydroxyl surface in potassium-acetate-intercalated kaolinite between 25 and 300° C, Langmuir 16 (2000) 7421–7428.
[29] L. Heller-Kallai, Reactions of salts with kaolinite at elevated temperatures, Clay Miner. 13 (1978) 221–235.
[30] M. Gabor, L. Poeppl, E. Koeros, Effect of ambient atmosphere on solid state reaction of kaolin-salt mixtures, Clays Clay Miner. 34 (1986) 529–533.
[31] M. Harish Bhat, M. Ganguli, K.J. Rao, Investigation of the mixed alkali effect in boro-tellurite glasses –the role of NBO–BO switching in ion transport, Curr. Sci. 86 (2004) 676.
[32] K.J. Rao, S. Kumar, Multialkali phosphate glasses: a new window to understand the mechanism of ion transport, Curr. Sci. 85 (2003) 945–955.
[33] S. Kumar, K.J. Rao, Dielectric relaxation in glasses: possible origin of the stretched relaxation behaviour, Chem. Phys. Lett. 387 (2004) 91–99.
[34] S. Kumar, K.J. Rao, Lithium ion transport in germanophosphate glasses, Solid State Ion. 170 (2004) 191–199.
[35] S. Kumar, P. Vinatier, A. Levasseur, K.J. Rao, Investigations of structure and transport in lithium and silver borophosphate glasses, J. Solid State Chem. 177 (2004) 1723–1737.
[36] O.L. Anderson, D.A. Stuart, Calculation of activation energy of ionic conductivity in silica glasses by classical methods, J. Am. Ceram. Soc. 37 (1954) 573–580.
[37] J.F.M. Oudenhoven, L. Baggetto, P.H.L. Notten, All-solid-state lithium-ion micro-batteries: a review of various three-dimensional concepts, Adv. Energy. Mater. 1 (2011) 10–33.
[38] M. Ferhi, K. Horchani-Naifer, K. Ben Saad, M. Férid, Modeling Li-ion conductivity in LiLa(PO3)4 powder, Physica B 407 (2012) 2593–2600.
[39] M. Férid, K. Horchani, A. Touati, A. Madani, H. Boussetta, M. Trabelsi-Ayadi, Étude des propriétés de conduction électrique des phosphates condensés mixtes éléments monovalents-terres rares: $liDy(PO_3)_4$ $NaNd(PO_3)_4$, $AgLa(PO_3)_4$, $NH_4Dy(PO_3)_4$, J. Phys. IVFr. 113 (2004) 115–118.
[40] H. Ettis, H. Naili, T. Mhiri, The crystal structure, thermal behaviour and ionic conductivity of a novel lithium gadolinium polyphosphate $LiGd(PO_3)_4$, J. Solid State Chem. 179 (2006) 3107.
[41] A. Jouini, M. Férid, A. Touati, M. Trabelsi-Ayadi, Préparation et étude des propriétés de conduction ionique des polyphosphate mixtes de type $M^{I}M^{III}(PO_3)_4$, (M^{I} = Li K et M^{III} = Y, Bi), J. Phys. IVFr. 113 (2004) 125–128.
[42] N. El Horr, A. Hammou, M. Bagieu, Etude des propriétés de conduction électrique des polyphosphates: $li_3Ba_2(PO_3)_7$, $LiPb_2(PO_3)_5$, $LiCs(PO_3)_2$, et αLiK $(PO_3)_2$, J. Solid State Chem. 90 (1991) 361–366.
[43] K. Horchani-Naifer, M. Férid, Structure and ionic conductivity of $NaCeP_2O_7$, Solid State Ion. 176 (2005) 1949–1953.